The Astrophysical Journal, 745:167 (5pp), 2012 February 1 doi:10.1088/0004-637X/745/2/167

THEORETICAL WAVELENGTHS OF Fe XVI L-SHELL TRANSITIONS AND COMPARISON WITH LABORATORY MEASUREMENTS AND *CHANDRA* OBSERVATIONS OF CAPELLA

P. Beiersdorfer[1], F. Diaz[2], and Y. Ishikawa[2]
[1] Physics Division, Lawrence Livermore National Laboratory, Livermore, CA 94550, USA
[2] Department of Chemistry and the Chemical Physics Program, University of Puerto Rico, San Juan, PR 00931, USA
Received 2011 May 15; accepted 2011 December 6; published 2012 January 16

ABSTRACT

We have used the relativistic multi-reference Møller–Plesset perturbation theory to calculate the energy levels of Fe XVI, including those of the autoionizing levels with a hole state in the L shell. Comparison of the resulting L-shell transition wavelengths with those from recent laboratory measurements shows remarkable agreement, i.e., agreement within the experimental uncertainties. Our calculation allows us to predict the wavelength of the second strongest $2p$–$3d$ Fe XVI line, which has not yet been directly observed in the laboratory, to be 15.266 Å. This wavelength is within 0.0042 Å of the strong Fe XVII line commonly labeled 3D. Relying on the high accuracy of our calculations, we have reassigned two previously identified lines and predict a different location than previously thought for the strongest Fe XVI magnetic quadrupole transition. Inspection of the spectra of Capella recorded with the transmission grating spectrometers on the *Chandra X-ray Observatory* yields features corresponding to the predicted location of the innershell excited Fe XVI lines. These features have not been identified before. Our analysis shows that these features are most likely from Fe XVI.

Key words: atomic processes – line: formation – stars: coronae – stars: individual (Capella) – Sun: X-rays, gamma rays – X-rays: general

Online-only material: color figures

1. INTRODUCTION

Accurate wavelengths are a prerequisite for fitting astrophysical spectra and extracting the information contained in superb spectra obtained with present-day observatories, such as the *Chandra* and *XMM-Newton* X-ray observatories (Brickhouse et al. 2000). Without accurate wavelengths, the fluxes from various lines, for example, may be incorrectly added in modeling spectra, resulting in faulty inferred parameters such as emission measures, temperatures, or densities.

Because of the importance of accurate wavelengths a large portion of laboratory astrophysics measurements have been dedicated to producing line lists with the best possible wavelengths (Beiersdorfer 2003; Lepson et al. 2008). In parallel, there have been multiple theoretical developments to produce wavelengths that match those produced by laboratory measurements and required by astrophysical observations. For example, a combination of the Many-Body Pertubation Theory (MBPT) method and the configuration-interaction (CI) method was used by Gu (2005) and Gu et al. (2006) to produce wavelengths of L-shell transitions in iron and nickel that were shown to be superior to earlier results using the CI method alone, as employed, for example, by the Hebrew University Lawrence Livermore Atomic Code (HULLAC; Bar-Shalom et al. 2001) or by the Flexible Atomic Code (FAC; Gu 2008). Similarly, exceptionally high accuracy on the order of 0.1% has been achieved in theoretical atomic structure calculations for Fe XIX by Kotochigova et al. (2007) using a combination of the CI method with second-order Brillouin–Wigner perturbation theory.

The relativistic multi-reference Møller–Plesset (MR–MP) perturbation theory (Ishikawa et al. 1991; Ishikawa & Vilkas 2001) has also been shown to produce exceptionally accurate wavelengths. For example, the transition energies calculated with this method for the L-shell transitions of Fe XVII were found to agree with measurements within the experimental uncertainties (Ishikawa et al. 2009). In the following we employ this method to calculate the L-shell transitions of Fe XVI.

L-shell transitions of M-shell ions have gained new prominence because they are observed in absorption in spectra from active galactic nuclei (Sako 2001; Holczer et al. 2007). The measurement of these lines in the laboratory has been difficult, making accurate calculations very important. With only one valence electron in the M shell, Fe XVI represents the simplest M-shell ion, and thus represents an ideal test case to apply our method to M-shell ions. Moreover, it is the only M-shell ion for which comprehensive laboratory data exist (Brown et al. 2001; Graf et al. 2009).

Our calculations allow us to make a prediction of the $(2p^5_{1/2}3s_{1/2}3d_{3/2})_{J=3/2} \rightarrow (2p^6 3s_{1/2})_{J=1/2}$ transition labeled C by Brown et al. (2001) and line "3" by Graf et al. (2009). This line blends with the $(2p^5_{1/2}3d_{3/2})_{J=1} \rightarrow (2p^6)_{J=0}$ Fe XVII line labeled 3D (Parkinson 1973). This Fe XVI line has so far not been measured in the laboratory because it appears to perfectly blend with the neon-like iron line within the resolution of the available spectrometers, both in the laboratory and in orbit.

Using our calculated wavelengths for the subset of Fe XVI lines observed by Graf et al. (2009) we have inspected the spectrum of Capella to check for features that may correspond to Fe XVI lines. We present this analysis in Section 4 below. We indeed find unassigned features in the spectrum of Capella that correspond to the location of the predicted Fe XVI lines. We predict lines beyond those observed by Graf et al. (2009) that are relevant to the analysis of astrophysical spectra and show that these correspond to the position of additional unassigned flux in the spectrum of Capella. Inclusion of the Fe XVI collisional innershell satellite lines will clearly improve future modeling fits of the spectrum of Capella, as well as that of other astrophysical sources of iron L-shell emission.

2. COMPUTATIONAL DETAILS

The atomic structure of the Fe^{15+} ion and the radiative transition rates connecting the energy levels were calculated using the relativistic MR–MP perturbation theory. An in-depth

Table 1
Comparison of Calculated with Measured Wavelengths of the Innershell Excited Fe XVI Transitions

Label[a]	Label[b]	λ_{exp}[c] (Å)	λ_{MR-MP}[d] (Å)	λ_{FAC}[c] (Å)	Identification[c]	Identification[d]	I (10^{-5} photons/s/ion)
1	A	15.111(4)	15.110	15.107	$(2p^63s)_{J=1/2} - (2p_{1/2}2p^4_{3/2}3s_{1/2}3d_{5/2})_{J=3/2}$	$(2p^63s)_{J=1/2} - (2p_{1/2}2p^4_{3/2}3s_{1/2}3d_{5/2})_{J=3/2}$	223
2a	B	15.19(2)	15.191	15.185	$(2p^63p_{3/2})_{J=3/2} - (2s_{1/2}2p^63s^2)_{J=1/2}$	$(2p^63p_{3/2})_{J=3/2} - (2s_{1/2}2p^63s^2)_{J=1/2}$	331
2b	B	15.210(4)	15.211	15.215	$(2p^63s)_{J=1/2} - (2p_{1/2}2p^4_{3/2}3s_{1/2}3d_{3/2})_{J=1/2}$	$(2p^63s)_{J=1/2} - (2p_{1/2}2p^4_{3/2}3s_{1/2}3d_{3/2})_{J=1/2}$	2375
3	C	15.261(3)	15.266	15.276	$(2p^63s)_{J=1/2} - (2p_{1/2}2p^4_{3/2}3s_{1/2}3d_{5/2})_{J=3/2}$	$(2p^63s)_{J=1/2} - (2p_{1/2}2p^4_{3/2}3s_{1/2}3d_{5/2})_{J=3/2}$	1550
4		15.516(5)	15.518	15.533	$(2p^63s)_{J=1/2} - (2p^2_{1/2}2p^3_{3/2}3s_{1/2}3d_{5/2})_{J=3/2}$	$(2p^63s)_{J=1/2} - (2p^2_{1/2}2p^3_{3/2}3s_{1/2}3d_{5/2})_{J=3/2}$	486
5		15.679(9)	15.678	15.703	$(2p^63s)_{J=1/2} - (2p^2_{1/2}2p^3_{3/2}3s_{1/2}3d_{3/2})_{J=3/2}$	$(2p^63s)_{J=1/2} - (2p^2_{1/2}2p^3_{3/2}3s_{1/2}3d_{3/2})_{J=3/2}$	134
6a		17.37(1)	17.371	17.404	$(2p^63s)_{J=1/2} - (2p^2_{1/2}2p^3_{3/2}3s^2)_{J=3/2}$	$(2p^63s)_{J=1/2} - (2p^2_{1/2}2p^3_{3/2}3s^2)_{J=3/2}$	46
6b		17.395(4)	17.398	17.426	$(2p^63d_{5/2})_{J=5/2} - (2p^2_{1/2}2p^3_{3/2}3s_{1/2}3d_{5/2})_{J=5/2}$	$(2p^63d_{5/2})_{J=5/2} - (2p^2_{1/2}2p^3_{3/2}3s_{1/2}3d_{5/2})_{J=5/2}$	23
			17.389	17.430	$(2p^63d_{3/2})_{J=3/2} - (2p_{1/2}2p^4_{3/2}3p^2_{3/2})_{J=3/2}$	$(2p^63d_{3/2})_{J=3/2} - (2p_{1/2}2p^4_{3/2}3p^2_{3/2})_{J=3/2}$	26
6c		17.417(4)	17.411	17.439	$(2p^63d_{5/2})_{J=5/2} - (2p^2_{1/2}2p^3_{3/2}3s_{1/2}3d_{5/2})_{J=7/2}$	$(2p^63d_{5/2})_{J=5/2} - (2p^2_{1/2}2p^3_{3/2}3s_{1/2}3d_{5/2})_{J=7/2}$	43
			17.419	17.449	$(2p^63d_{3/2})_{J=3/2} - (2p^2_{1/2}2p^3_{3/2}3s_{1/2}3d_{3/2})_{J=3/2}$	$(2p^63d_{3/2})_{J=3/2} - (2p^2_{1/2}2p^3_{3/2}3s_{1/2}3d_{3/2})_{J=3/2}$	79
7		17.447(4)	17.435	17.473	$(2p^63p_{1/2})_{J=1/2} - (2p^2_{1/2}2p^3_{3/2}3s_{1/2}3p_{3/2})_{J=3/2}$	$(2p^63p_{1/2})_{J=1/2} - (2p^2_{1/2}2p^3_{3/2}3s_{1/2}3p_{3/2})_{J=3/2}$	28
			17.452	17.481	$(2p^63d_{3/2})_{J=3/2} - (2p^2_{1/2}2p^3_{3/2}3s_{1/2}3d_{3/2})_{J=5/2}$	$(2p^63d_{3/2})_{J=3/2} - (2p^2_{1/2}2p^3_{3/2}3s_{1/2}3d_{3/2})_{J=5/2}$	55
			17.451	17.485	$(2p^63p_{3/2})_{J=3/2} - (2p^2_{1/2}2p^3_{3/2}3s_{1/2}3p_{3/2})_{J=1/2}$	$(2p^63p_{3/2})_{J=3/2} - (2p^2_{1/2}2p^3_{3/2}3s_{1/2}3p_{3/2})_{J=1/2}$	115
8a		17.494(6)	17.474	17.513	$(2p^63p_{1/2})_{J=1/2} - (2p^2_{1/2}2p^3_{3/2}3s_{1/2}3p_{1/2})_{J=1/2}$	$(2p^63p_{1/2})_{J=1/2} - (2p^2_{1/2}2p^3_{3/2}3s_{1/2}3p_{1/2})_{J=1/2}$	67
			17.487	17.516	$(2p^63d_{5/2})_{J=5/2} - (2p^2_{1/2}2p^3_{3/2}3s_{1/2}3d_{3/2})_{J=7/2}$	$(2p^63d_{5/2})_{J=5/2} - (2p^2_{1/2}2p^3_{3/2}3s_{1/2}3d_{3/2})_{J=7/2}$	56
			17.493	17.535	$(2p^63d_{5/2})_{J=5/2} - (2p^2_{1/2}2p^3_{3/2}3s_{1/2}3d_{5/2})_{J=5/2}$	$(2p^63d_{5/2})_{J=5/2} - (2p^2_{1/2}2p^3_{3/2}3s_{1/2}3d_{5/2})_{J=5/2}$	273
			17.495	17.537	$(2p^63p_{3/2})_{J=3/2} - (2p^2_{1/2}2p^3_{3/2}3s_{1/2}3p_{3/2})_{J=3/2}$	$(2p^63p_{3/2})_{J=3/2} - (2p^2_{1/2}2p^3_{3/2}3s_{1/2}3p_{3/2})_{J=3/2}$	87
			17.500	17.541	$(2p^63p_{1/2})_{J=1/2} - (2p^2_{1/2}2p^3_{3/2}3s_{1/2}3p_{3/2})_{J=5/2}$	$(2p^63p_{1/2})_{J=3/2} - (2p^2_{1/2}2p^3_{3/2}3s_{1/2}3p_{3/2})_{J=5/2}$	149
8b		17.510(4)	17.512	17.552	$(2p^63p_{1/2})_{J=1/2} - (2p^2_{1/2}2p^3_{3/2}3s_{1/2}3p_{1/2})_{J=3/2}$	$(2p^63p_{1/2})_{J=1/2} - (2p^2_{1/2}2p^3_{3/2}3s_{1/2}3p_{1/2})_{J=3/2}$	127
		NA[e]	17.577			$(2p^63p_{3/2})_{J=3/2} - (2p^2_{1/2}2p^3_{3/2}3s_{1/2}3p_{3/2})_{J=7/2}$	564
9a		17.592(4)	17.597	17.619	$(2p^63p_{3/2})_{J=3/2} - (2p^2_{1/2}2p^3_{3/2}3s_{1/2}3p_{3/2})_{J=7/2}$	$(2p^63p_{1/2})_{J=3/2} - (2p^2_{1/2}2p^3_{3/2}3s_{1/2}3p_{1/2})_{J=5/2}$	154
9b		17.612(6)	17.615	17.638	$(2p^63p_{1/2})_{J=3/2} - (2p^2_{1/2}2p^3_{3/2}3s_{1/2}3p_{1/2})_{J=5/2}$	$(2p^63p_{1/2})_{J=1/2} - (2p^2_{1/2}2p^3_{3/2}3s_{1/2}3p_{1/2})_{J=3/2}$	58
9c		17.633(7)		17.656	$(2p^63p_{1/2})_{J=1/2} - (2p^2_{1/2}2p^3_{3/2}3s_{1/2}3p_{1/2})_{J=3/2}$	no corresponding Fe XVI line	
10		17.678(3)	17.680	17.721	$(2p^63p_{3/2})_{J=3/2} - (2p^2_{1/2}2p^3_{3/2}3s_{1/2}3p_{1/2})_{J=3/2}$	$(2p^63p_{3/2})_{J=3/2} - (2p^2_{1/2}2p^3_{3/2}3s_{1/2}3p_{1/2})_{J=3/2}$	264

Notes.
[a] Used by Graf et al. (2009).
[b] Used by Brown et al. (2001).
[c] From Graf et al. (2009).
[d] This work.
[e] No wavelength assigned or feature observed at this location by Graf et al. (2009).

derivation of the theory and procedures used is described by Ishikawa et al. (1991) and Ishikawa & Vilkas (2001). Details for the calculations of transition probabilities are provided by Vilkas & Ishikawa (2005).

The relativistic MR–MP atomic physics computer program may be subdivided into three parts: (1) an initial state-averaged multi-configuration Dirac–Fock calculation (MCDF) to obtain a set of spinors for (2) the subsequent multi-reference configuration-interaction calculation (MR-CI). The final part (3) is the actual, level-specific MR–MP perturbation theory calculation.

The state-averaged second-order MCDF equation yields a well-balanced set of spinors suitable for describing the ground and even- and odd-parity core-excited (γ,$\mathcal{J}$,π) levels. For Fe XVI, the MCDF calculation was performed using single excitation of an electron from the $3s$ shell to $n\ell$ ($n = 4$, 5 and $\ell = s$, $p_{1/2}$, $p_{3/2}$, $d_{3/2}$, $d_{5/2}$, $f_{5/2}$, or $f_{7/2}$). Thus, the state-averaged MCDF includes a total of 19 configuration-state functions (CSF) of even and odd parity with $\mathcal{J} = 1/2$–$7/2$, arising from the $1s^22s^22p^63s^1$ through $1s^22s^22p^65f^1$ configurations, to determine a single set of spinors for the MR-CI and MR–MP calculations that follow.

In order to account for strong configuration mixing among the quasi-degenerate open-shell states, the MR-CI for the ground and core-excited $\mathcal{J} = 1/2$–$11/2$ states in the Na-like ion were subsequently carried out, including the core-excited configurations $2s^m2p^n3\ell^p3\ell'^q$, with $m + n + p + q = 9$ and $p + q \leqslant 2$. The CI eigenvectors were used to evaluate the frequency-dependent Breit interaction, normal mass shift, and the specific mass shift, which were evaluated as first-order corrections along with the Lamb shifts (Ishikawa & Vilkas 2001). Each of the MR-CI eigenstates was then subjected to state-specific relativistic MR–MP refinement to account for the residual dynamic correlation to second order of perturbation theory.

The large and small radial components of the Dirac spinors were expanded in sets of even-tempered Gaussian-type functions (Ishikawa et al. 1991) that satisfy the boundary conditions associated with the finite nucleus (Ishikawa et al. 1991). Even-tempered basis sets of $30s28p26d24f22g22h$ G spinors (G for "Gaussian") for up to angular momentum $L = 5$, and 15 G spinors for $L = 6$–11 are employed. The order of the partial-wave expansion L_{max}, the highest angular momentum of the spinors included in the virtual space, is $L_{max} = 11$ throughout this study. The nuclei were simulated as spheres of uniform proton charge with the radii $R(\text{Bohr}) = 2.2677 \times 10^{-5}A^{1/3}$, where A is atomic mass (amu).

Radiative probabilities for electric dipole (E1), electric quadrupole (E2), magnetic dipole (M1), and magnetic quadrupole (M2) transitions were calculated between all the levels. In Table 1 we list the transition energies of the Fe XVI transitions observed in the laboratory and deemed relevant to contribute to the L-shell emission spectra of astrophysical sources by earlier calculations (Graf et al. 2009) of the

Table 2
Calculated Wavelengths of Additional Innershell Excited Fe XVI Transitions

Label	λ_{FAC} (Å)	λ_{MR-MP} (Å)	Identification	I (10^{-5} photons/ion/s)
11	15.214	15.236	$(2p^6 3p_{3/2})_{J=3/2} - (2s2p^6 3s^2)_{J=1/2}$	25
12	15.510	15.487	$(2p^6 3s)_{J=1/2} - (2s^2 2p_{1/2}^2 2p_{3/2}^3 3s3d_{5/2})_{J=1/2}$	30
13	16.965	16.937	$(2p^6 3p_{3/2})_{J=3/2} - (2p_{1/2}2p_{3/2}^4 3s3p_{3/2})_{J=3/2}$	42
14	16.960	16.953	$(2p^6 3d_{3/2})_{J=3/2} - (2s^2 2p_{1/2}2p_{3/2}^4 3s3d_{3/2})_{J=1/2}$	47
15	17.044	17.029	$(2p^6 3d_{5/2})_{J=5/2} - (2p_{1/2}2p_{3/2}^4 3s3d_{5/2})_{J=3/2}$	50
16	17.143	17.126	$(2p^6 3d_{3/2})_{J=3/2} - (2s^2 2p_{1/2}2p_{3/2}^4 3s3d_{3/2})_{J=5/2}$	31
17a	17.160	17.131	$(2p^6 3p_{1/2})_{J=1/2} - (2s^2 2p_{1/2}^2 2p_{3/2}^3 3s3p_{3/2})_{J=3/2}$	34
17b	17.160	17.131	$(2p^6 3d_{5/2})_{J=5/2} - (2p_{1/2}2p_{3/2}^4 3s3d_{5/2})_{J=7/2}$	71
17c	17.151	17.134	$(2p^6 3d_{5/2})_{J=5/2} - (2p_{1/2}2p_{3/2}^4 3s3d_{3/2})_{J=5/2}$	59
18	17.186	17.160	$(2p^6 3d_{3/2})_{J=3/2} - (2p_{1/2}2p_{3/2}^4 3s3d_{5/2})_{J=5/2}$	52
19	17.221	17.193	$(2p^6 3p_{3/2})_{J=3/2} - (2p_{1/2}^2 2p_{3/2}^3 3s3p_{3/2})_{J=3/2}$	46
20a	17.246	17.210	$(2p^6 3p_{3/2})_{J=3/2} - (2p_{1/2}2p_{3/2}^4 3s3p_{3/2})_{J=5/2}$	118
20b	17.248	17.209	$(2p^6 3p_{1/2})_{J=1/2} - (2p_{1/2}2p_{3/2}^4 3s3p_{1/2})_{J=3/2}$	103
21a	17.273	17.233	$(2p^6 3p_{3/2})_{J=3/2} - (2p_{1/2}2p_{3/2}^4 3s3p_{3/2})_{J=3/2}$	103
21b	17.276	17.245	$(2p^6 3p_{3/2})_{J=3/2} - (2p_{1/2}^2 2p_{3/2}^3 3s3p_{3/2})_{J=5/2}$	53
22	17.365	17.344	$(2p^6 3d_{5/2})_{J=5/2} - (2p_{1/2}^2 2p_{3/2}^3 3s3d_{5/2})_{J=3/2}$	107

predicted line intensities. In Table 2 we list additional Fe XVI transitions. These have not been reported by Graf et al. (2009). However, these lines are predicted to have intensities similar to those reported by Graf et al. (2009) and thus should also be of relevance to astrophysical spectra. In order to determine the expected line intensities, we have constructed a collisional-radiative model with FAC (Gu 2008). The calculations were carried out at a density of 10^{10} cm^{-3} and an electron temperature of 228 eV ($\log T = 6.42$ MK), which corresponds approximately to the temperature of maximum abundance of Fe^{15+} ions (Bryans et al. 2006). Our model included all collisional processes connecting the Fe XVI ground state to the $2s^2 2p^5 3\ell^2$ excited states as well as all excited states to each other. The predicted intensities are listed in Tables 1 and 2. We chose a lower cutoff of 2.3×10^{-4} photon s^{-1} emitted by an Fe XVI ion, corresponding to the intensity of a line that is part of feature 6*b* and the weakest transition reported by Graf et al. (2009), for including transitions in the tables.

A listing of all calculated energy levels and associated radiative transition rates obtained in our MR–MP calculations will be given elsewhere (F. Diaz et al. 2012, in preparation).

3. COMPARISON WITH LABORATORY MEASUREMENTS AND PRIOR IDENTIFICATIONS

In Table 1 we also list the energies and identifications of the Fe XVI transitions provided by the two recent laboratory measurements (Brown et al. 2001; Graf et al. 2009) as well as the transition energies given by Graf et al. (2009) that were calculated using FAC. A comparison of the laboratory measurements and our calculations shows excellent agreement. In fact, it is remarkable that the agreement is within the uncertainty limits of the measurements for all measured features. In cases where a measured feature is a blend of multiple lines, the calculated wavelength of the strongest contributor is in agreement with the measured wavelength. There is one exception, i.e., line C. This line blends with the Fe XVII line 3D and has not been observed directly in the laboratory. The discrepancy between experiment and theory is no need for concern, as the uncertainty associated with the measurement is that of the position of (the blended) line 3D and not that of line C.

Such excellent agreement, as displayed by the results in Table 1, has eluded earlier calculations. The wavelengths from FAC, for example, which were shown by Graf et al. (2009) to be in much better agreement with the measurements than any of the prior calculations, differ roughly by 5–10 times the wavelength uncertainty of the measurements, i.e., as much as 0.043 Å.

3.1. Revised Line Identifications

The excellent agreement between our calculations and measurements gives us confidence to revise three of the earlier identifications.

Feature 9a was thought to be formed by the $(2p^6 3p_{3/2})_{J=3/2} - (2p_{1/2}^2 2p_{3/2}^3 3s_{1/2}3p_{3/2})_{J=7/2}$ transition, which is a magnetic quadrupole transition. We identify this feature instead as the electric dipole allowed $(2p^6 3p_{1/2})_{J=3/2} - (2p_{1/2}^2 2p_{3/2}^3 3s_{1/2}3p_{1/2})_{J=5/2}$ transition.

The M2 line, which was predicted by FAC to be sizeable enough to be seen and thought to correspond to feature 9a, is instead located at 17.577 Å according to our calculations. Inspection of the crystal spectrometer data provided by Graf et al. (2009) shows a possible feature at this location, which was, however, not assigned. More measurements will probably be needed to clearly identify this feature, especially since it appears to be absent in their grating spectrum.

Feature 9b was thought to be formed by the $(2p^6 3p_{1/2})_{J=3/2} - (2p_{1/2}^2 2p_{3/2}^3 3s_{1/2}3p_{1/2})_{J=5/2}$ transition. Based on our calculations, this transition forms feature 9a, as discussed above. Feature 9b is formed instead by the $(2p^6 3p_{1/2})_{J=1/2} - (2p_{1/2}^2 2p_{3/2}^3 3s_{1/2}3p_{1/2})_{J=3/2}$ transition.

Graf et al. (2009) assigned the $(2p^6 3p_{1/2})_{J=1/2} - (2p_{1/2}^2 2p_{3/2}^3 3s_{1/2}3p_{1/2})_{J=3/2}$ transition to the shoulder of one of their observed features at 17.633(7) Å based on the FAC wavelength of 17.656 Å. We calculate the wavelength of this line to be 17.615 Å and identify it with feature 9b, as discussed

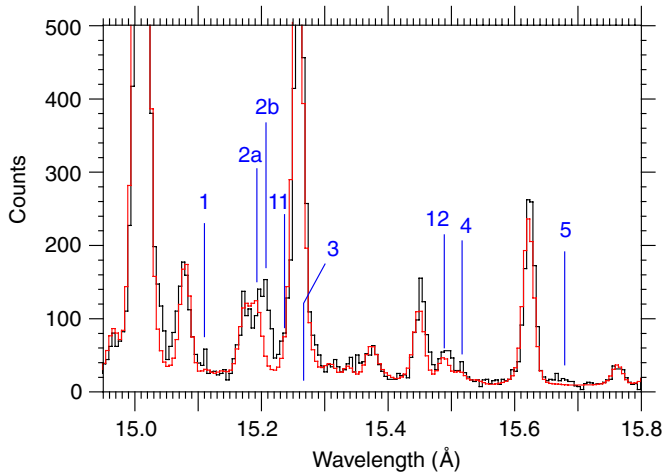

Figure 1. Spectrum of Capella in the region 14.9–15.8 Å produced by co-adding 596 ks of observations collected with *Chandra*'s medium energy grating (MEG) in +1 order (black trace). Also shown is a fit of the spectrum (red trace) based on known spectral lines. The positions of the Fe XVI lines, as calculated by the MR–MP method, are indicated and labeled in the notation used in Tables 1 and 2.

(A color version of this figure is available in the online journal.)

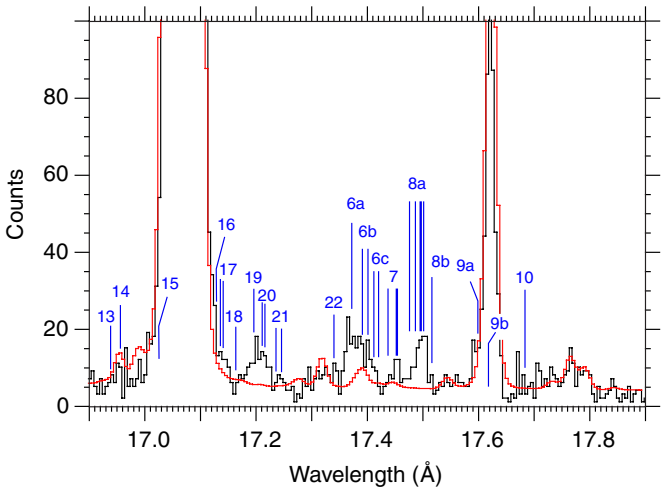

Figure 2. Spectrum of Capella in the region 16.9–17.9 Å produced by co-adding 596 ks of observations collected with *Chandra*'s medium energy grating (MEG) in +1 order (black trace). Also shown is a fit of the spectrum (red trace) based on known spectral lines. The positions of the Fe XVI lines, as calculated by the MR–MP method, are indicated and labeled in the notation used in Tables 1 and 2.

(A color version of this figure is available in the online journal.)

above. We do not predict an Fe XVI line that would be situated at the measured wavelength of 17.633(7) Å. This shoulder in the laboratory spectra may have been spurious, or it may possibly be caused by a different charge state of iron.

Finally, one of the transitions contributing to feature 8a was listed by Graf et al. (2009) as $(2p^6 3p_{1/2})_{J=1/2} - (2p_{1/2}^2 2p_{3/2}^3 3s_{1/2} 3p_{3/2})_{J=5/2}$. This would make it another magnetic quadrupole transition, but no discussion of such an unusual transition was given. We think that this was likely a typographical mistake in the total angular momentum of the ground level, as we predict an E1 transition that terminates in the $(2p^6 3p_{1/2})_{J=3/2}$ level.

3.2. The Feature at 15.26 Å

As we have already mentioned, the only wavelength for which we differ with the laboratory measurements of Graf et al. (2009) is the wavelength of the $(2p^6 3s)_{J=1/2} - (2p_{1/2} 2p_{3/2}^4 3s_{1/2} 3d_{5/2})_{J=3/2}$ transition. The experimental wavelength is dominated by the Fe XVII line 3D. Graf et al. (2009) give the wavelength of the blend as 15.261(3) Å. Brown et al. (1998) give the wavelength of the (probably nearly) Fe XVI-free feature as 15.261(2) Å, while Beiersdorfer & Wargelin (1994) give the wavelength of this line as 15.265(2) Å.

Using the MR–MP method, Ishikawa et al. (2009) have calculated the wavelength of the 3D line to be 15.2614 Å. This value agrees very well with the most recent two laboratory measurements. The predicted splitting between the Fe XVI line C, for which we calculate a wavelength of 15.2656 Å, and the Fe XVII line 3D is thus 0.0042 Å. A spectrometer with a resolving power $\lambda/\Delta\lambda \geqslant 3600$ will be needed to split the two lines apart. This by far exceeds the resolving powers of current instrumentation, including that of *Chandra*'s high energy transmission grating spectrometer.

4. Fe XVI EMISSION FROM CAPELLA

The identification of Fe XVI lines in astrophysical spectra has been difficult. The reason has been that standard spectral analysis codes do not (yet) include collisional lines from Fe XVI (and those from lower charge states of iron). The Astrophysical Plasma Emission Code (APEC) described by Smith et al. (2001), for example, currently does not include Fe XVI lines produced by electron-impact excitation. (Note that APEC does include some Fe XVI lines produced by dielectronic recombination, but this list is not complete (Beiersdorfer et al. 2012).)

Confirmation of laboratory evidence (Brown et al. 2001) that Fe XVI lines play an important role in blending with the Fe XVII line 3D was reported in an analysis of solar data (Brickhouse & Schmelz 2006). However, even before then, Behar et al. (2001) using a spectral model generated with the HULLAC already pointed out the importance of blends with Fe XVI lines. Among the two $n = 3 \rightarrow n = 2$ Fe XVI transitions listed among their identifications, one was thought to be blended with the O VIII Lyγ line at 15.176 Å; the other was thought to be blended with the Fe XVII 3D line at 15.261 Å. The latter was described as the $(2p^6 3s)_{J=1/2} - (2p_{1/2} 2p_{3/2}^4 3s_{1/2} 3p_{3/2})_{J=3/2}$ transition, which would mean that it is a magnetic dipole transition and rather unlikely. This may have been a typographical error, where $3d_{5/2}$ was mistakenly replaced by $3p_{3/2}$. In that case, the line would be identical to line C, which indeed blends with 3D. The former transition was described as the $(2p^6 3s)_{J=1/2} - (2p_{1/2} 2p_{3/2}^4 3s_{1/2} 3d_{3/2})_{J=3/2}$ transition with a wavelength given as 15.188 Å. This transition corresponds to one of the two lines contributing to feature B, i.e., the line labeled 2b by Graf et al. (2009). But instead of contributing to the oxygen Lyγ feature at 15.181 Å, as proposed in the analysis of Behar et al. (2001), this line is, according to our calculations, located at 15.211 Å and can be readily identified in the Capella spectrum, as shown below.

In Figures 1 and 2 we show spectra of Capella in the 14.9–15.8 Å and 16.9–17.9 Å wavelength regions. The spectra were produced by co-adding 596 ks of observations collected with *Chandra*'s medium energy grating (MEG) in +1 order. The spectrum in Figure 1 is dominated by the strong Fe XVII line commonly referred to as 3C at 15.01 Å. The second strongest feature is that of line 3D at 15.26 Å. The spectrum in Figure 2 is dominated by the two strong Fe XVII lines commonly referred

to as 3G and M2 at 17.05 Å. The second strongest feature is that of an Fe XVIII line at 17.62 Å (Drake et al. 1999).

The Capella spectra have been fitted using APEC, which was modified for emissivities and wavelengths as described by Gu (2009). This fit is shown in the two figures. Because APEC does not include collisional Fe XVI transitions, there should be excess flux in the observed spectra in the locations of the strongest Fe XVI lines that is not reproduced by the fit. To aid identification of such excess flux, we have marked the location of the Fe XVI transitions predicted by our calculations in both figures.

Inspection of the two figures indeed shows excess flux that can be attributed to the Fe XVI transitions listed in Tables 1 and 2. In fact, this excess flux is rather substantial. Similar amounts of excess flux at the location of the collisional Fe XVI lines are also seen in the MEG −1 order spectra as well as in the +1 and −1 order HEG spectra. In other words, each spectrum produced by either plus or minus order from each type of grating contains excess flux at the location of the Fe XVI lines. This makes us very confident that the excess flux is real and that the Fe XVI lines provide a significant contribution to the Capella line emission.

The strongest Fe XVI feature is formed by lines 2a and 2b. They produce the unfitted flux around 15.2 Å, i.e., the long-wavelength part of the double-humped feature situated near this wavelength. The short-wavelength half of the feature is clearly associated with the Lyγ line of O VIII. The long-wavelength half can be attributed only in part to an L-shell line in Fe XIX leaving the excess flux seen in Figure 1. The Fe XVI lines 2a and 2b (or feature B in the notation of Brown et al. 2001) are the most suitable candidate lines left. Identifying the long-wavelength part of the 15.2 Å feature as Fe XVI emission was also suggested by Gu (2009).

The other candidate Fe XVI lines in this wavelength region are lines 1, 3, 4, and 5. Each of these lines, except line 3 (or line C in the notation of Brown et al. 2001) can be attributed to excess flux in the spectrum. Line 3, of course, is blended with the Fe XVII line 3D and cannot be resolved. Lines 11 and 12 have not been reported by Graf et al. (2009) and their predicted intensities are small. However, especially line 12 appears to match well with unfitted flux in the Capella spectra near 15.5 Å.

The experiments of Graf et al. (2009) showed that the Fe XVI emission in the 17–18 Å region is much weaker than that near 15 Å. This is confirmed in our collisional-radiative modeling calculation and is also seen in the Capella spectra. The flux level in Figure 2 is much lower than that in Figure 1.

Although the flux level is weak, the 17–18 Å spectral band contains notable, unfitted emission. Fe XVI lines appear to account for essentially all of the unfitted flux in the wavelength region from 17.1 to 17.7 Å. The Fe XVI features 6a, 6b, and 6c match the broad unfitted Capella flux near 17.37 Å. Feature 7 matches the unfitted peak near 17.45 Å, and 8a and 8b match the distinct unfitted feature at 17.5 Å. Line 9b is blended with the Fe XVIII line at 17.62 Å and cannot be identified; however, line 9a appears to correspond to the short-wavelength shoulder of the strong Fe XVIII line. Line 10 appears to match the flux at 17.675 Å.

The substantial, broad feature around 17.2 Å cannot be accounted for by the lines reported by Graf et al. (2009). However, our calculations show that there are several Fe XVI features, which we label 19, 20, and 21, that could readily form this broad feature. Lines 16, 17, and 18 appear to contribute to the unfitted flux on the long-wavelength shoulder of the strong Fe XVII line near 17.1 Å. We also note that there is little evidence in the Capella spectra for the presence of the Fe XVI M2 line at 17.577 Å predicted by the FAC calculations of Graf et al. (2009) as well as by our modeling predictions.

5. CONCLUSION

We have shown that our calculations predict very accurate wavelengths for the strongest collisional Fe XVI lines. Our calculations give a prediction of the separation of the Fe XVII line 3D and the Fe XVI line with which it blends. In particular, the splitting is predicted to be a mere 0.0042 Å. The two lines can thus only be resolved with instrumentation that has a resolving power of $\lambda/\Delta\lambda = 3600$ or better.

We have identified the corresponding Fe XVI emission features in the *Chandra* spectra of Capella. The lines appear to account for the unfitted flux in the 15–16 Å and 17–18 Å region.

Given the excellent agreement between our calculated wavelengths with those measured in the laboratory, the MR–MP calculations hold good promise for calculating accurate wavelengths of other, more complex M-shell iron ions in the future.

Work by the Lawrence Livermore National Laboratory was performed under the auspices of the Department of Energy under Contract No. DE-AC52-07NA-27344. This work was supported by NASA Astronomy and Physics Research and Analysis contract NNG07WF05I and Chandra Research Award AR1-12006X. We are very grateful to Dr. Ming Feng Gu for providing us with copies of the summed and fitted Capella spectra and thank Mr. Maximilian Bode for preparing part of the figures and tables.

REFERENCES

Bar-Shalom, A., Klapisch, M., & Oreg, J. 2001, J. Quant. Spectrosc. Radiat. Transfer, 71, 179
Behar, E., Cottam, J., & Kahn, S. M. 2001, ApJ, 548, 966
Beiersdorfer, P. 2003, ARA&A, 41, 343
Beiersdorfer, P., Gu, M. F., Lepson, J. K., & Desai, P. 2012, Astr. Soc. Pac., TBD, in press
Beiersdorfer, P., & Wargelin, B. J. 1994, Rev. Sci. Instrum., 65, 13
Brickhouse, N. S., Dupree, A. K., Edgar, R. J., et al. 2000, ApJ, 530, 387
Brickhouse, N. S., & Schmelz, T. J. 2006, ApJ, 636, L53
Brown, G., Beiersdorfer, P., Kahn, S., Liedahl, D., & Widmann, K. 1998, ApJ, 502, 1015
Brown, G. V., Beiersdorfer, P., Chen, H., Chen, M. H., & Reed, K. J. 2001, ApJ, 557, L75
Bryans, P., Badnell, N. R., Gorczyca, T. W., et al. 2006, ApJS, 167, 343
Drake, J. J., Swartz, D. A., Beiersdorfer, P., Brown, G. V., & Kahn, S. M. 1999, ApJ, 521, 839
Graf, A., Beiersdorfer, P., Brown, G. V., & Gu, M. F. 2009, ApJ, 695, 818
Gu, M. F. 2005, ApJS, 156, 105
Gu, M. F. 2008, Can. J. Phys., 86, 675
Gu, M. F. 2009, arXiv:0905.0519
Gu, M. F., Holczer, T., Behar, E., & Kahn, S. M. 2006, ApJ, 641, 1227
Holczer, T., Behar, E., & Kaspi, S. 2007, ApJ, 632, 788
Ishikawa, Y., López Encarnación, J. M., & Träbert, E. 2009, Phys. Scr., 79, 025301
Ishikawa, Y., Quiney, H. M., & Malli, G. L. 1991, Phys. Rev. A, 63, 3270
Ishikawa, Y., & Vilkas, M. J. 2001, Phys. Rev. A, 63, 042506
Kotochigova, S., Kirby, K. P., & Tupitsyn, I. 2007, Phys. Rev. A, 76, 052513
Lepson, J., Beiersdorfer, P., Bitter, M., & Kahn, S. M. 2008, Can. J. Phys., 86, 175
Parkinson, J. H. 1973, A&A, 24, 215
Sako, M. 2001, A&A, 365, L168
Smith, R. K., Brickhouse, N. S., Liedahl, D. A., & Raymond, J. C. 2001, ApJ, 556, L91
Vilkas, M. J., & Ishikawa, Y. 2005, Phys. Rev. A, 72, 032512